ACS Photonics

Article

pubs.acs.org/journal/apchd5

Nonstoichiometric SiC Bus/Ring Waveguide Based All-Optical Data Format Follower and Inverter

Sheng-Pin Su,[†] Chung-Lun Wu,[†,‡] Chih-Hsien Cheng,[†] Bo-Ji Huang,[†] Huai-Yung Wang,[†] Cheng-Ting Tsai,[†] Yung-Hsiang Lin,[†] Yu-Chieh Chi,[†] Min-Hsiung Shih,[§,∥] Chao-Kuei Lee,[‡] and Gong-Ru Lin*[,†]

[†]Graduate Institute of Photonics and Optoelectronics, and Department of Electrical Engineering, National Taiwan University (NTU), No. 1, Roosevelt Road Sec. 4, Taipei 10617, Taiwan, Republic of China

[‡]Department of Photonics and Department of Physics, National Sun Yat-sen University, No. 70, Lien-Hai Rd., Kaohsiung 804, Taiwan, Republic of China

[§]Department of Photonics and Institute of Electro-Optical Engineering, National Chiao Tung University, 1001 Ta Hsueh Road, Hsinchu 30010, Taiwan, Republic of China

[∥]Research Center for Applied Sciences, Academia Sinica, Taipei 11529, Taiwan, Republic of China

ABSTRACT: Nonstoichiometric silicon carbide (SiC) bus/ring waveguide resonator based all-optical data-format follower and inverter is demonstrated to perform ultrafast dual-functional wavelength and data-format conversion. The buried Si quantum dots (Si-QDs) with strong quantum confinement effect effectively result in a significant change on the nonlinear refractive index of 3.14×10^{-13} cm^2/W, which induces a red-shift of 0.07 nm on the resonant wavelength comb of the nonstoichiometric SiC ring waveguide resonator. By injecting the 12 Gbit/s optical pulsed return-to-zero on−off keying (PRZ-OOK) data stream into the ring waveguide at a notched wavelength of 1551.08 nm, the induced red-shift on resonant wavelengths allows versatile all-optical data processing functions, including data wavelength conversion and data format following/inversion, on the data patterns transferred to the probe. The eye-opening diagram analysis at 12 Gbit/s reveals that the data transferred to the probe can provide a signal-to-noise ratio of 9.4 dB, and a receiving power penalty is degraded by 2.6 dB as compared to that of the pump data.

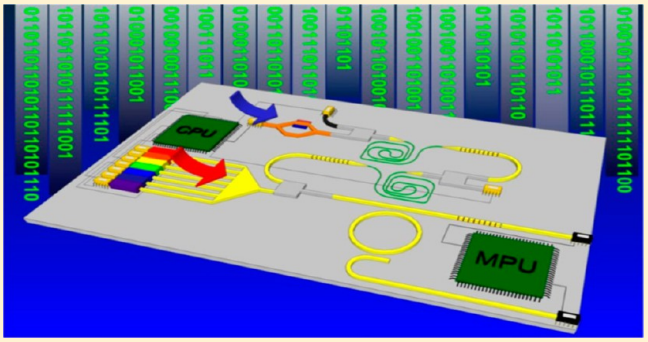

KEYWORDS: *nonstoichiometric SiC, ring waveguide resonator, nonlinear Kerr effect, all-optical data inverter*

All-optical integrated switching devices fabricated on Si bench have recently been comprehensively investigated due to its potential application in the future high-speed communication systems. With the use of free-carrier absorption (FCA) effect at early stage, the all-optical modulation in the Si quantum dot doped Si-rich silicon oxide (SiO_x:Si-QD) waveguide has been reported previously.[1−4] However, the switching speed of such functional devices based on the FCA effect is limited by the relatively long free-carrier lifetime, which is ∼1 ns for bulk Si or ∼1 μs for Si-QD.[4] In particular, the modulation depth and switching speed are compromised each other when the size of the Si-QD is determined. To achieve the high-speed data transmission in the near future, the alternative approach that induced by nonlinear optical effect is considered at current stage. Recently, the nonlinear Kerr effect induced all-optical data processing in the SiO_x:Si-QD based slot waveguide was also demonstrated.[5] With the presence of the buried nanoscale Si-QD in the SiO_2 host matrix, the nonlinear refractive index arises much higher than that of the standard SiO_2. Such an enhancement on the optical nonlinearity can be predicted by the quantum confinement effect.[6−9] However, the low refractive index of SiO_x:Si-QD based device usually results in an extremely high coupling loss without specific design on the waveguide geometry.[3,5] In addition, the nonlinear Kerr switch made by bulk Si waveguide always suffers from the two photon absorption effect due to its low energy bandgap.[10] The SiN_x material is employed as an alternative to replace the Si material. Lin et al. utilized the Si-rich SiN_x based Kerr switch to process the data conversion at a data rate of more than 10 Gbit/s.[11] However, the observed nonlinear refractive index for the Si-rich SiN_x material is only 3.14×10^{-13} cm^2/W, indicating that the higher peak power of the pump data is necessary for obtaining the larger group index change. From this point of view, the nonstoichiometric silicon carbide (SiC) is recently considered as one of the potential candidates. The nonstoichiometric SiC has been extensively investigated for different applications such as light-emitting diodes (LEDs),[12−15] solar cells,[16−19] and detectors.[20−23]

Received: January 8, 2016
Published: April 19, 2016

DOI: 10.1021/acsphotonics.6b00016
ACS Photonics 2016, 3, 806−818

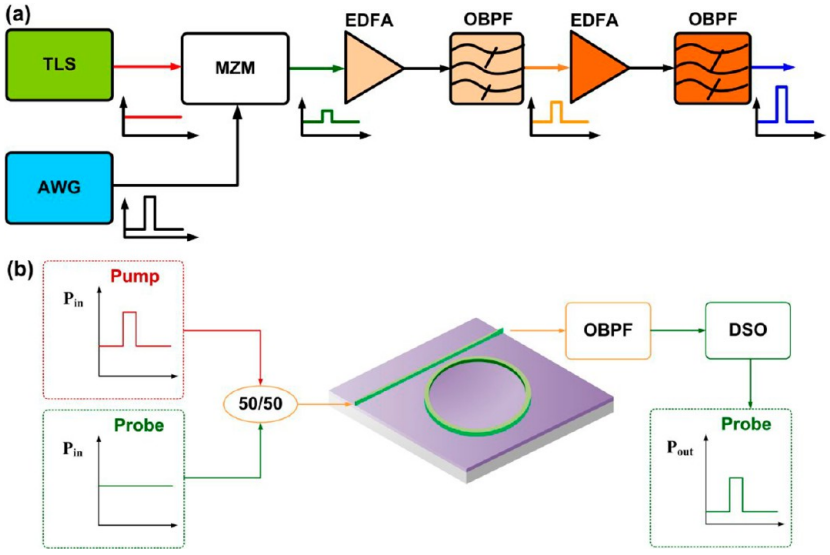

Figure 1. (a) System setup for the optical PRZ-OOK data-stream generation by encoding the AWG delivered electrical PRZ-OOK data-stream onto the single-mode optical carrier through the external intensity modulator. (b) Pump−probe system for implementing the nonlinear Kerr switch.

Benefiting from the relatively wide bandgap energy (E_g, for the commonly encountered polymorph of a-SiC E_g = 3.05 eV) and high thermal stability,[24] the nonstoichiometric SiC offers a low absorption coefficient and a high optical damage threshold, which is suitable for high-power operation. Moreover, the nonstoichiometric SiC is predicted to exhibit high nonlinear refractive index at optical telecommunication wavelengths; however, there is lack of literature discussing the transient variation on the nonlinear refractive index of nonstoichiometric SiC at near-infrared wavelengths.[25]

In this work, the high-speed all-optical data follower and inverter operated under a pulsed return-to-zero on−off keying (PRZ-OOK) format of up to 12 Gbit/s is demonstrated by using a nonstoichiometric SiC based bus/ring waveguide resonator. With the transient wavelength red-shift occurred on the periodically notched transmittance spectrum of the nonstoichiometric SiC based bus/ring waveguide resonator, the nonlinear refractive index of the nonstoichiometric SiC around 1550 nm is preliminarily determined. Due to the ultrafast response of the nonlinear Kerr effect, the nonlinear refractive index inside the bus/ring waveguide resonator is transiently modified by the optical pulsed data pattern, which simultaneously causes the red-shift on resonant wavelengths of the ring waveguide. This eventually leads to a high-speed all-optical cross-wavelength modulation of up to 12 Gbit/s accompanying a format sign preserved data when probing at on-resonant wavelength and a format sign inverted data when probing at off-resonant wavelength.

METHODS

Generation of Intense Optical Pulsed Data-Stream Based Pump for Determining Kerr Coefficient and Switching Responses. For testing the data-format follower and inverter based on the nonstoichiometric SiC ring waveguide resonator, a single-mode laser pulsated by an external intensity modulator driven with a PRZ formatted data patterns is employed as the incoming source, as shown in Figure 1a. To obtain the PRZ data pattern, a homemade computer program generated PRZ data pattern with a pattern length of 2^7-1 and a peak-to-peak amplitude of 1.5 V is loaded into a commercial arbitrary waveform generator (AWG). A wavelength tunable single-mode laser passes through the integrated intensity modulator which is DC-biased at linear transfer regime (V_{bias} = 0.5 V_π + V_{offset} ~ 4.5 V) and RF driven by the electrical PRZ data pattern concurrently. The optical PRZ data pattern is amplified to enlarge its peak power through two sets of in-line and boost optical amplifiers, and a narrow band optical filter with a pass bandwidth of 0.4 nm is inserted in between for intensity noise suppression.

The pump−probe system for demonstrating the nonlinear optical Kerr effect based data-format follower and inverter is shown in Figure 1b. Another continuous-wave laser is employed as the probe source with its wavelength tunable between adjacent notch transmittance points of the transfer function of the nonstoichiometric SiC ring resonator. Both the continuous-wave optical probe signal at on- or off-resonant dip wavelength and the pulsated optical pump signal located exactly at notch transmittance of the transfer function are concurrently inserted into the nonstoichiometric SiC bus/ring waveguide via a 50/50 1 × 2 coupler in connection with a lensed fiber. After passing through the nonstoichiometric SiC bus/ring waveguide, another optical bandpass filter screens out the pump component but leaves the probe component with data-format followed or inverted PRZ pattern for receiving and decoding at remote node. A commercially available optical receiver with built-in trans-impedance linear amplifier detects the format followed or inverted data pattern, which is cross-wavelength converted from pump to probe, and the eye-diagram of the detected electrical data waveform is characterized with a wide-bandwidth communication analyzer mainframe and its high-speed plug-ins.

RESULTS AND DISCUSSION

Material Preparation and Structural Analysis. The nonstoichiometric SiC film was deposited on a 3-μm thick SiO_2 coated Si wafer by using the plasma-enhanced chemical vapor deposition (PECVD) process. During growth, a gaseous mixture of argon diluted silane (90% Ar+10% SiH_4) and methane (CH_4) is employed as the recipe, and the chamber temperature and pressure are maintained at 550 °C and 134 Pa, respectively. With a RF plasma power of 120 W, the fluence ratio was

DOI: 10.1021/acsphotonics.6b00016
ACS Photonics 2016, 3, 806−818

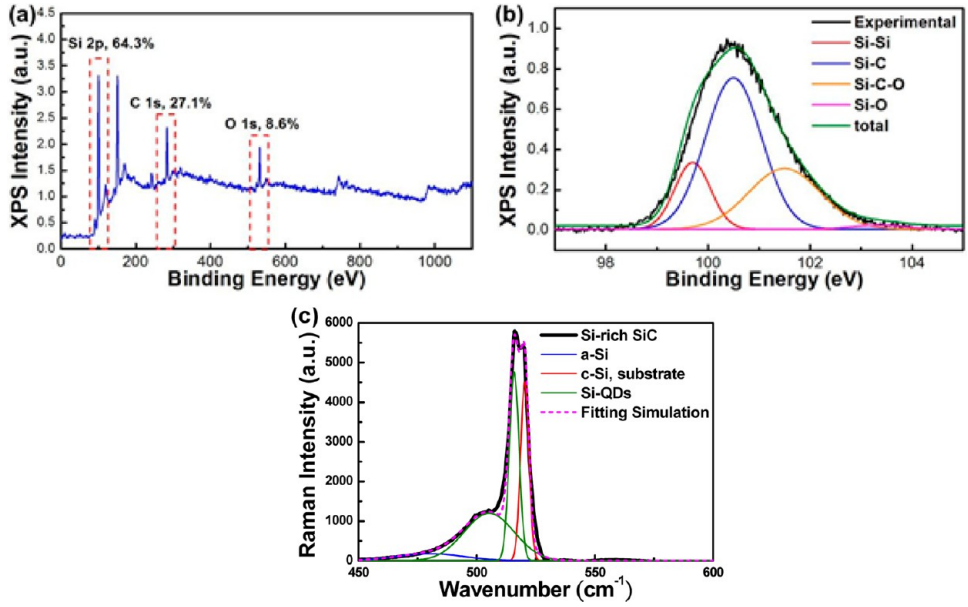

Figure 2. (a) Full-band XPS analysis, (b) compositional bonding components decomposed from the $Si_{(2p)}$ XPS spectrum, and (c) Raman scattering spectrum of the nonstoichiometric SiC:Si-QD film.

controlled at $R = [CH_4]/([SiH_4] + [CH_4]) = 0.5$ to facilitate the growth of nonstoichiometric SiC. To avoid the influence of dopants on the Kerr effect, the intrinsic nonstoichiometric SiC layer was fabricated during the growth, which contributes to a resistivity of 10 MΩ·cm. To characterize the composition ratio and the crystallinity of the nonstoichiometric SiC, the analyses of the X-ray photoelectron spectroscopy (XPS) and the Raman scattering spectroscopy (RSS) are performed.

Figure 2a illustrates the complete XPS spectrum for characterizing the composition ratio of the nonstoichiometric SiC film. The atomic concentrations of Si and C are obtained as 64.3% and 27.1%, respectively. In comparison with the standard SiC (with a Si/C composition ratio of 50%), the nonstoichiometric SiC grown with $R = 0.5$ enlarges its excessive concentration up to 37.2%. This gives a nonstoichiometric $SiC_{0.42}$ matrix. Furthermore, the decomposition of the component peak is performed. Figure 2b shows that the $Si_{(2p)}$ contributed XPS spectral peak consists of four individual bonding components including the Si−Si at bonding energy of 99.7 eV, the Si−C at bonding energy of 100.5 eV, the C−Si−O at bonding energy of 101.5 eV, and the O−Si−O at bonding energy of 103.35 eV.[26] The presence of the Si−Si bond is supporting evidence for the existence of buried Si-QDs in the nonstoichiometric SiC host matrix. In addition, the Raman spectroscopy clearly shows the crystallinity of the buried Si-QDs which is self-assembled from the excessive Si atoms in the nonstoichiometric SiC host matrix, as shown in Figure 2c. Except the Raman scattering peak at 520 cm^{-1} contributed by the single-crystalline Si wafer, there are broadened side pedestals below 520 cm^{-1} contributed by Si-QDs[27,28] with different sizes of 2−3 nm (confirmed by high-resolution transmission electron microscope (HRTEM) analysis). In view of the observed HRTEM Si-QD image and the line width broadened Raman spectra related to the polycrystalline Si-QDs, the line width broadening of Si-QD related Raman scattering can considerably be attributed to both the diverse size distribution and the finite nonzero phonon divergence in the Si-QDs.[29]

In more detail, the HRTEM and the selected area diffraction (SAD) analyses were performed to deduce whether there are nanoscale polycrystalline Si precipitates or not. As a result, the cross-sectional bright-field HRTEM image confirms the existence of polycrystalline Si-QDs buried in the nonstoichiometric SiC host matrix, as shown in Figure 3a, in which the

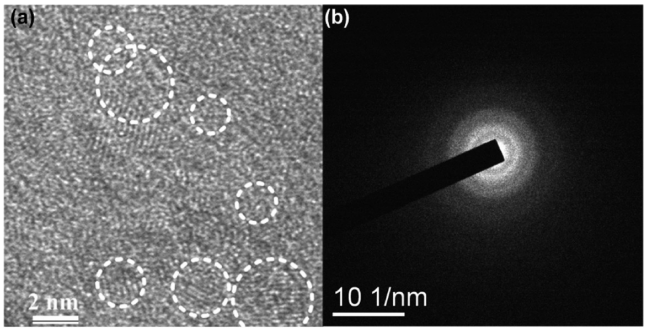

Figure 3. (a) TEM image and the (b) SAD pattern of the Si-QDs embedded in nonstoichiometric SiC film.

circled regions reveal that the diameter of these precipitated polycrystalline Si-QD is about 2−3 nm with a lattice constant of about 0.194 nm. In addition, the SAD pattern of these Si-QDs embedded in nonstoichiometric SiC shown in Figure 3b also presents clear diffraction rings, which provides the corresponding *d*-spacings of 0.313 and 0.196 nm for (111)- and (220)-oriented crystalline lattices in Si-QDs, respectively.

Device Design, Fabrication, and Characterization. To determine the ring waveguide geometry, the refractive index of the nonstoichiometric SiC film was fitted by the analytic results of the surface reflectance. With the Si-QD doped in the nonstoichiometric SiC host matrix, the refractive index of nonstoichiometric SiC slightly increases to ∼2.63 at near-infrared wavelengths by fitting with the simulation curve, as shown in Figure 4a. Afterward, a commercially available software (Rsoft) with the beam propagation method (BPM) based numerical simulation tool is utilized to analyze the field distribution of the single transverse mode in the nonstoichiometric SiC channel waveguide sandwiched by SiO_2 at the top and

DOI: 10.1021/acsphotonics.6b00016
ACS Photonics 2016, 3, 806−818

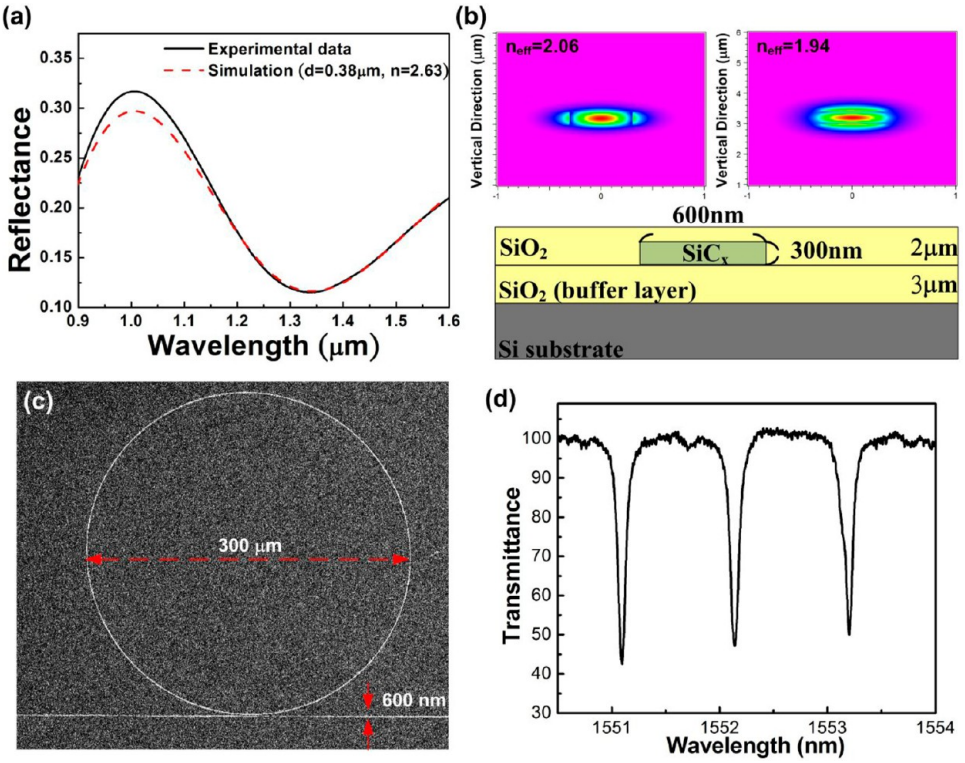

Figure 4. (a) Experimental (solid) and simulated (dashed) reflectance spectra for extracting the effective refractive index. (b) The transverse mode profiles with effective indices for TE_0 and TM_0 modes. Right lower inset: the schematic diagram for the SiO_2 sandwiched nonstoichiometric SiC channel waveguide on Si substrate. (c) Top-view image of the nonstoichiometric SiC channel bus/ring waveguides on the SiO_2/Si substrate. (d) Periodically notched transmission spectrum of the nonstoichiometric SiC ring waveguide resonator.

bottom. During the simulation, the refractive indices of SiO_2, nonstoichiometric SiC, and Si are set as 1.46, 2.63, and 3.5, respectively. Under single-mode operation, the waveguide width and height are 600 and 300 nm, respectively. Figure 4b shows the mode distributions of TE_0 and TM_0 modes with corresponding effective indices of 2.067 and 1.94, respectively. In experiment, the in-line polarizer is employed to maintain the TE-mode incidence with a TE/TM polarization mode extinction ratio of 25 dB.

For fabricating the nonstoichiometric SiC bus and ring channel waveguides, the electron-beam writer exposures the positive photoresist to define the bus/ring waveguide pattern at initial stage. Subsequently, the metallic Cr film was evaporated upon the photoresist layer to serve as a dry-etching mask. After lithographic lift-off patterning the waveguide geometry in developer, the inductively coupled plasma reactive-ion etching (ICP-RIE) of the mask covered nonstoichiometric SiC substrate under a gaseous mixture of oxygen (O_2) and trifluoromethane (CHF_3) was formed to etch out the unpatterned non-stoichiometric SiC for the waveguide formation. The top-view image of the SiC bus/ring waveguide taken by scanning electron microscopy (SEM) is shown in Figure 4c. After etching the metallic mask, a stoichiometric SiO_2 layer with a film thickness of 2 μm synthesized by standard PECVD is employed as the up-cladding layer of the nonstoichiometric SiC waveguide. Then, both input and output facets of the bus waveguide were polished to reduce the coupling loss of the bus waveguide to be smaller than 3 dB/facet. With the presence of the ring waveguide resonator, the output transmission power is periodically minimized with a dark-comb-like throughput transfer function on the notched transmission spectrum, as shown in Figure 4d. The quality factor as high as Q = 22800 and the transmittance drop of nearly 60% at a wavelength of 1551.08 nm is obtained with a spacing of $\delta\lambda$ = 1.04 nm.

The SEM images reveal the end-face and coupling structures of the nonstoichiometric SiC bus/ring waveguide, as shown in Figure 5. Figure 5a shows the complete SEM image of the whole

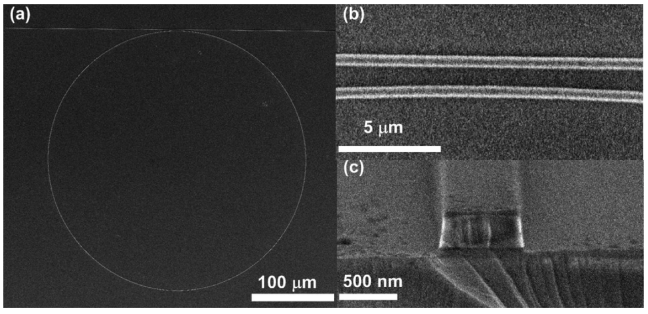

Figure 5. Top-view SEM images of (a) the nonstoichiometric SiC ring waveguide resonator and (b) the gap between the bus and ring wavegudes; (c) the cross-section-view SEM image of the non-stoichiometric SiC ring waveguide resonator.

ring waveguide resonator. The radius of ring waveguide is enlarged to 150 μm for reducing the bending loss. In more detail, the gap of the spacing between the straight bus and ring waveguides is only 700 nm, as shown in Figure 5b. Furthermore, Figure 5c further shows the cross-section-view SEM image of the nonstoichiometric SiC ring waveguide resonator. To enhance the coupling efficiency, the waveguide width at both ends is inversely tapered from 600 to 200 nm so as to form the 200 μm long inversed tapered couplers.

DOI: 10.1021/acsphotonics.6b00016
ACS Photonics 2016, 3, 806−818

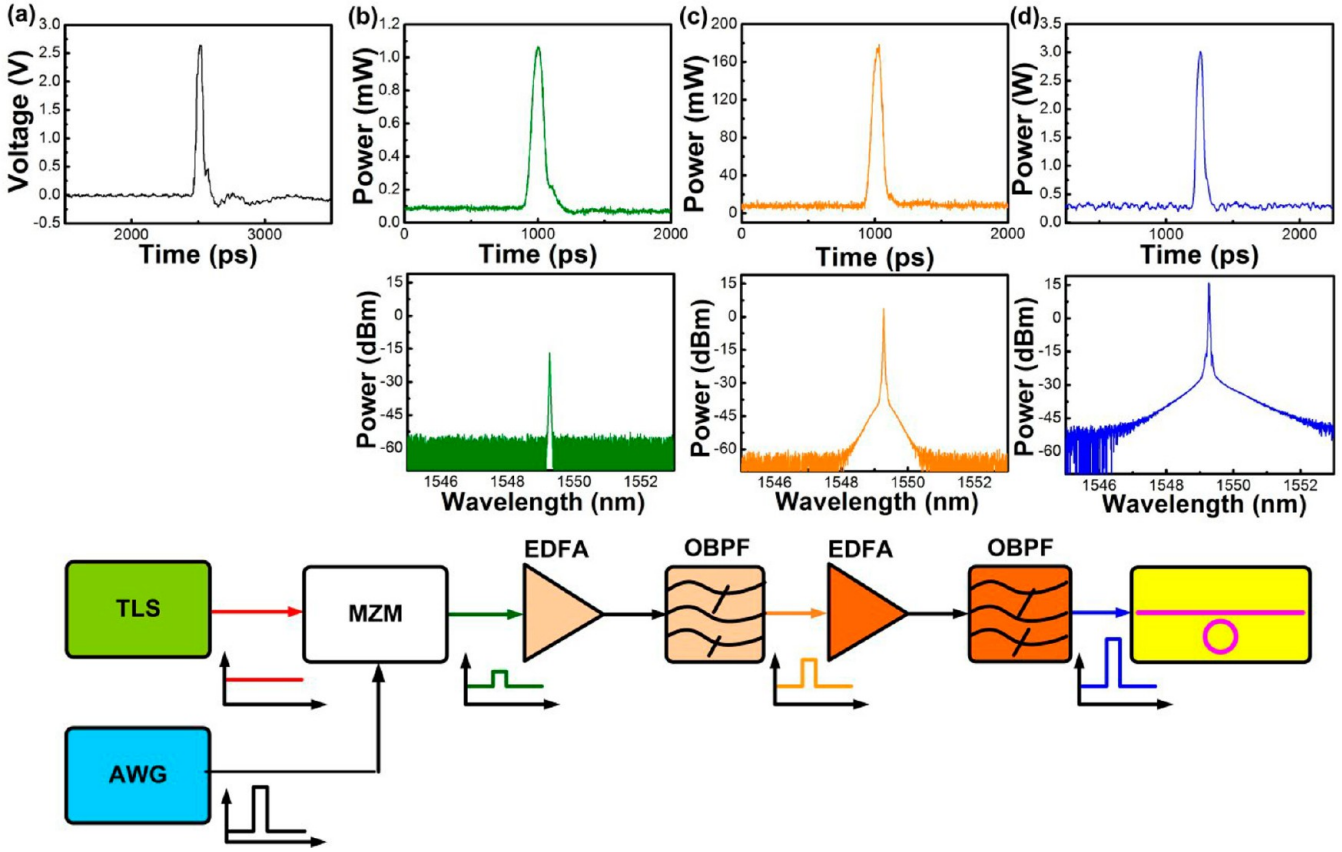

Figure 6. (a) Electrical pulse delivered from the AWG. (b) Pulse shape and spectrum of the modulated pump signal. (c) First-stage EDFA amplified pulse shape and spectrum of modulated pump signal. (d) Second-stage boost-amplified pulse shape and spectrum of modulated pump signal.

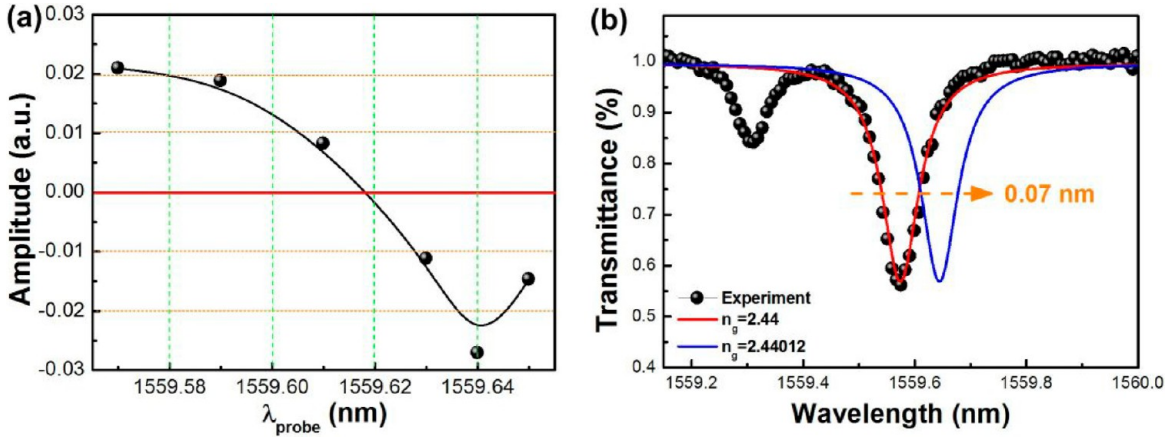

Figure 7. (a) Sign and amplitude of the cross-wavelength modulated probe signal as a function of wavelength. (b) Simulated notch spectra of transmission in the ring waveguide resonator without and with pulsed pumping.

Characterization on the Nonlinear Refractive Index of the Nonstoichiometric SiC. Figure 6 shows the time-domain traces and wavelength-domain spectra of the externally modulated pump beam monitored by the digital sampling oscilloscope for characterizing the optical Kerr coefficient and the nonlinear refractive index, which are transiently changed in the bus/ring waveguide under the existence of an intensive pump. The pulsed electrical data-stream with pulse duration of 80 ps and a repetition frequency of 12 MHz is employed, as shown in Figure 6a.

Then, a pump beam delivered from the tunable laser source (TLS) at a wavelength of 1551.08 nm is encoded by the electrical pulse through the Mach−Zehnder modulator to form the pump pulse-train with a peak power of 1 mW, as shown in Figure 6b. Afterward, Figure 6c shows the pulse-shape and spectrum of the first-stage optical pulse with a peak power as large as 180 mW. Finally, a second-stage amplification via a boost EDFA is necessary for enhancing the peak power of the pulsed optical pump data bit up to 3 W, with its pulse shape and spectrum shown in Figure 6d.

When scanning the wavelength of probe signal from on-resonance to off-resonance beneath the notch point of the nonstoichiometric SiC ring waveguide resonator, Figure 7a records the amplitude of the inverted modulated probe signals at

DOI: 10.1021/acsphotonics.6b00016
ACS Photonics 2016, 3, 806−818

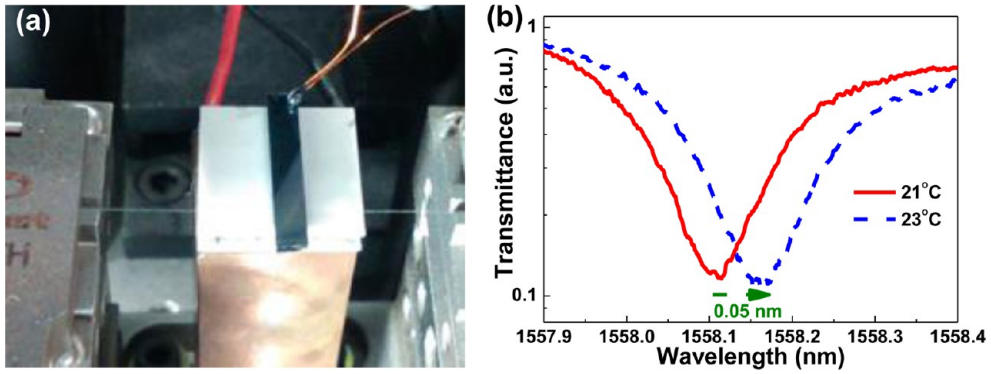

Figure 8. (a) Experimental setup for the temperature-stabilized nonstoichiometric SiC ring waveguide resonator. (b) Transmission spectra of nonstoichiometric SiC-based ring waveguide resonator at different temperatures.

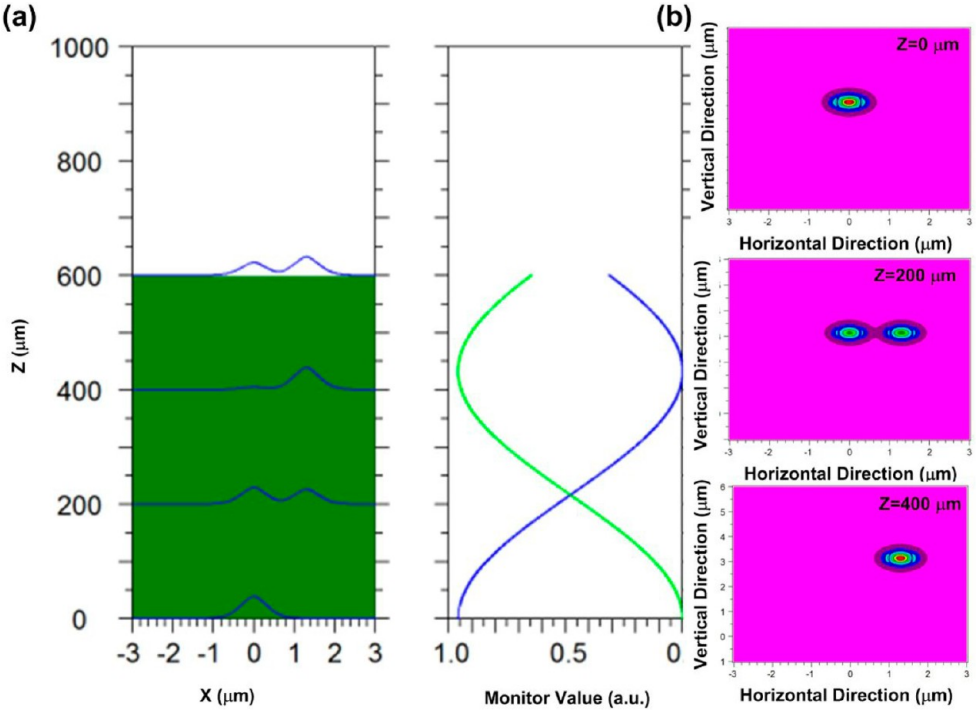

Figure 9. (a) BPM simulation traces on the coupling length (left) needed for the nonstoichiometric SiC bus/ring waveguide and (b) the mode profile extracted at different propagation distances of $z = 0$ μm (up), 200 μm (middle), and 400 μm (bottom).

different probe wavelengths. As observed from the experiment, the modulation amplitude is gradually degraded to zero when detuning the wavelength of probe away from the original notch point of the transfer function, however, which changes its sign and conversely enlarges its amplitude if further detunes apart from the original notch. Such a data-inversion phenomenon periodically occurs as the probe wavelength gradually approaches the next notch point in the transfer spectrum of the nonstoichiometric SiC ring waveguide resonator. From wavelength shift of the maximal data-inverted probe signal, the red-shift on the wavelength of ring resonance induced by the nonlinear Kerr effect is obtained as large as 0.07 nm. To declare the mechanism for cross-wavelength data follower and inverter, the section is divided into two parts of discussions. From the red-shifted wavelength of resonance dip caused by nonlinear Kerr effect in the nonstoichiometric SiC ring waveguide resonator, the nonlinear refractive index of the nonstoichiometric SiC can be determined by analyzing the resonance wavelength shift. Theoretically, the red-shifted transmittance of the ring waveguide resonator caused by the nonlinear refractive index change is expressed by

$$T(\lambda) = (1-\gamma)\left[1 - \frac{(1-x^2)(1-y^2)}{(1-xy)^2 + 4xy\,\sin^2(\pi(n_g + \Delta n_g)L_{cir}/\lambda)}\right] = (1-\gamma)\left[1 - \frac{(1-x^2)(1-y^2)}{(1-xy)^2 + 4xy\,\sin^2(\pi(n_g + n_2 I_{cir})L_{cir}/\lambda)}\right] \quad (1)$$

where γ and n_g represent the insertion-loss coefficient and the group refractive index, the parameters $x = (1-\gamma)^{0.5}\exp(-\alpha_{cir}L_{cir})$ and $y = \cos(\kappa l_i)$ are obtained from the theory of the ring waveguide resonator.[30] The red-shifted notch point at $\lambda + \delta\lambda$ is achieved by the change of group refractive index $n_g + \delta n_g \equiv n_g + n_2 I_{cir}$. Figure 7b shows the experimental and simulated transmittance spectra before and after experiencing the transient pump induced change on group refractive index owing to the Kerr effect.

DOI: 10.1021/acsphotonics.6b00016
ACS Photonics 2016, 3, 806−818

Figure 8a shows the photograph of a feedback temperature controlled scheme used in our experiment, which is constructed by allocating the nonstoichiometric SiC based ring waveguide resonator sample upon a thermoelectric cooler (TEC) plate controlled with a temperature stabilizer (ILX Lightwave, LDC-3724B). With the use of a thermistor directly adhered on the top surface of the sample substrate, the device temperature can be accurately detected and feedback to the temperature stabilizer. Under a precise control of temperature within ±0.1 °C, the temperature-dependent transmission spectra of the nonstoichiometric SiC-based ring waveguide resonator are shown in Figure 8b. As expected, the resonance-related dip in transmission spectra red-shifts its wavelength by 0.05 nm within a temperature increment of 2 °C (from 21 to 23 °C) due to the thermo-optic effect.[31] During the demonstration of all-optical data processing experiments, the temperature of the nonstoichiometric SiC-based ring waveguide resonator was precisely controlled at a desired temperature without variation (less than ±0.1 °C due to system limitation). In that case, the temperature variation induced resonance shift is merely $\sim 10^{-3}$ nm (with a corresponding slope of only 25 pm/°C), which is much smaller than that induced by the Kerr effect in the nonstoichiometric SiC-based ring waveguide resonator. Furthermore, the response time of the thermo-optic effect in Si and SiC is typically >10 μs,[32,33] which is much longer than the Kerr effect switching response.[34] Therefore, the ultrafast all-optical modulation with a bite rate of ∼10 Gbit/s in the nonstoichiometric SiC-based ring waveguide resonator is mainly originated from the nonlinear Kerr effect, and the thermo-optic effect induced slow switching response can be neglected in this case.

When scanning the wavelength of probe across the dip wavelength of the notched transfer function of the ring waveguide resonator, the pumping induced red-shift on the resonant dip of the transmittance spectrum can be fitted to be as large as 0.07 nm for the nonstoichiometric SiC ring waveguide resonator, indicating that the group refractive index change of 1.2×10^{-4} is induced by the product of pump intensity and nonlinear Kerr coefficient Note that the peak intensity of the pump signal (defined as $I_{cir} = M \times I_{pump}$) is slightly enlarged in the nonstoichiometric SiC ring waveguide at wavelength of resonance with its magnification described as[35]

$$M = \left| \frac{j \sin(\kappa' l_i) e^{-\alpha_{cir}/2L_{cir}}}{-\cos(\kappa' l_i) e^{-\alpha_{cir}/2L_{cir}} + e^{-j\theta}} \right|^2 \quad (2)$$

where α_{cir} denotes the propagation loss coefficient of nonstoichiometric SiC, κ' is the coupling coefficient of bus/ring waveguide, l_i is the bus/ring interaction length, L_{cir} is the length of ring waveguide, and θ is the round-trip phase deviation. To calculate the magnification factor M, the coupling coefficient between two directional coupler κ' have to be numerically analyzed by the beam propagation method, as shown in Figure 9.

In principle, the coupling coefficient (κ') between bus/ring waveguides can be expressed by $\kappa' = \pi/2L_c$, where L_c denotes the coupling length for 100% power transfer. For example, by setting the interaction gap width as 700 nm between the waveguides with identical width and height of 600 and 300 nm, respectively, the coupling length (L_c) is obtained as 430 μm, with a corresponding coupling coefficient of $\kappa' = 3.4 \times 10^{-3}$ μm^{-1}. During the single-trip propagation, the phase-shift of the optical filed inside the ring waveguide resonator must be an integral multiple of 2π. By fitting the measured probe transmittance spectrum with the theoretical transmittance function, the propagation loss coefficient of the ring waveguide resonator α_{cir} and interaction length l_i can be extracted from eq 1, as listed in Table 1. With these parameters derived from eq 1, the magnification factor M of the circulated intensity in the ring waveguide resonator ($M = I_{cir}/I_{input}$) turns out to be 1.157.

Table 1. Relative Parameters of Nonstoichiometric SiC Ring Waveguide Resonator

α_r (μm^{-1})	κ' (μm^{-1})	l_i (μm)	L_r (μm)	n_g
3.7×10^{-4}	0.0034	70	100π	2.44

By setting the peak incident pump power as 3 W in a 50/50 coupler with 5 dB coupling loss, the enhance peak intensity inside the ring waveguide resonator is $I_{cir} = P_{cir}/A_{eff} = 3.81 \times 10^8$ W/cm^2. Therefore, the nonlinear refractive index of the nonstoichiometric SiC at 1550 nm wavelengths is calculated as $n_2 = \delta n_g / I_{cir} = 3.14 \times 10^{-13}$ cm^2/W. During calculation, the group index is set as the same as the refractive index of nonstoichiometric SiC material. When comparing with the conventional bulk SiC, the nonstoichiometric SiC exhibits a nonlinear refractive index measured at 1550 nm, with 2 orders of magnitude larger than that of the bulk SiC measured at a wavelength of 785 nm.[36] Note that the nonlinear refractive index at shorter wavelengths is usually several magnitudes larger than that at longer wavelengths. With the presence of nanoscale Si-QDs, the third-order nonlinear susceptibility $\chi^{(3)}$ is enhanced due to the strong oscillation between the excitons. The significantly increased oscillation eventually results in a reduction of the Bohr radius. In fact, the third-order nonlinear susceptibility $\chi^{(3)}$ shows an inverse proportionality with sixth power of the Bohr radius, as following equation:[37]

$$\chi^{(3)} = \frac{16}{\pi \hbar^3} |p_{cv}|^4 |\varphi_{1s}(0)|^4 \frac{L R_0^2}{\lambda_{01}^4} \times \frac{\omega_0}{[\omega^2 - \omega_0^2][(3\omega)^2 - \omega_0^2]} \times \left[1 + \frac{4\omega^2}{\omega^2 - \omega_0^2}\right] \quad (3)$$

$$\varphi_{1s}(r) = \left[\frac{1}{\pi a^3}\right]^{1/2} e^{-r/a} \quad (4)$$

That is, the Si-QD doped in the nonstoichiometric SiC matrix results in a huge enhancement in n_2, which effectively favors the nonlinear optical Kerr switching in the nonstoichiometric SiC-based waveguide. For comparison, the open- and close-aperture Z-scan traces of stoichiometric and nonstoichiometric SiC films are shown in Figure 10. For the open-aperture Z-scan analysis of nonstoichiometric SiC, its transmittance near the focal point is significantly reduced, indicating the occurrence of two photon absorption (TPA) effect in Si-QDs buried in the nonstoichiometric SiC host matrix. The nonstoichiometric SiC shows a nonlinear absorption with a coefficient of -3.7×10^{-10} cm/W with fitting its open-aperture Z-scan trace, whereas the stoichiometric SiC does not exist a significant TPA effect.

The nonlinear refractive indices of stoichiometric and nonstoichiometric SiC can be obtained by fitting the close/open Z-scan traces shown in the lower part of Figure 10 with the modeled transmittance

DOI: 10.1021/acsphotonics.6b00016
ACS Photonics 2016, 3, 806−818

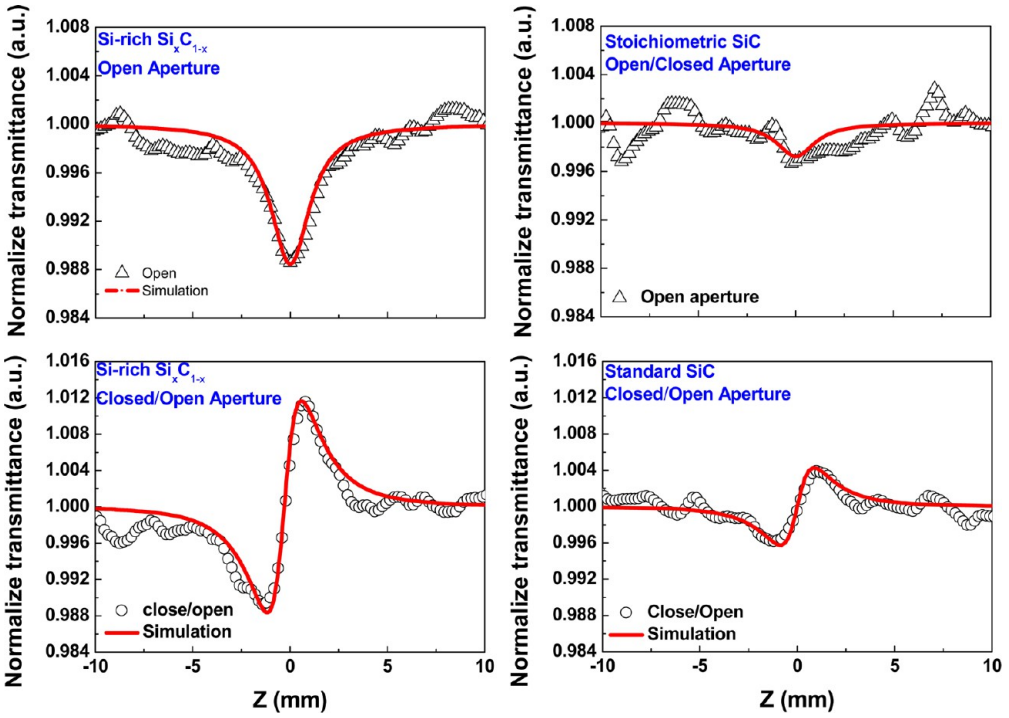

Figure 10. Open-aperture (upper row) and close-aperture (lower row) *Z*-scan traces of the Si-rich (left column) and the stoichiometric (right column) SiC films.

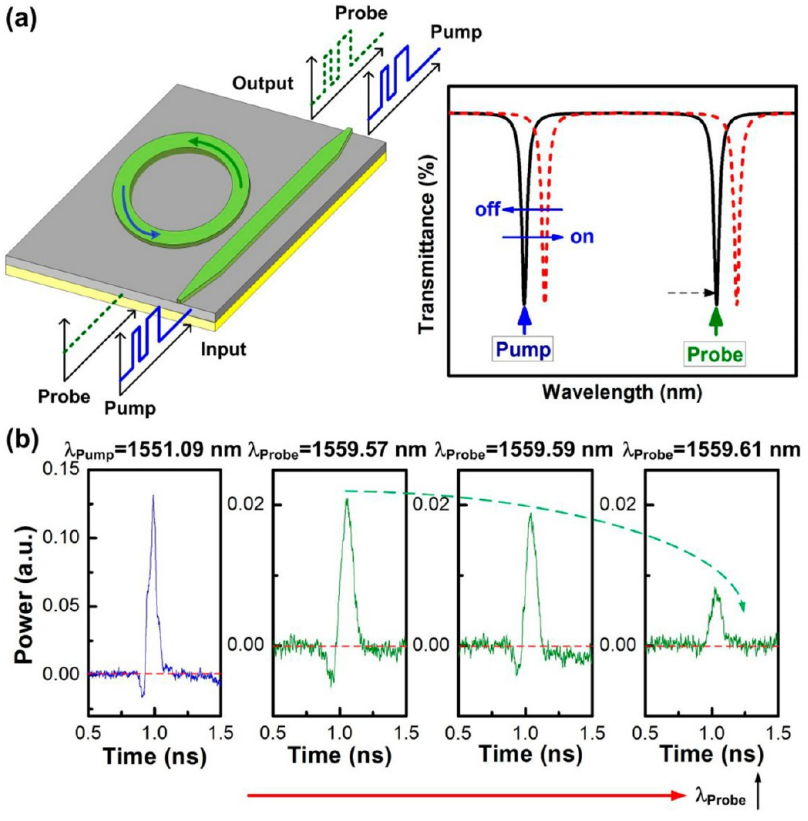

Figure 11. (a) Illustration on the operating principle of the wavelength conversion of the format preserved data-stream induced by nonlinear Kerr effect after passing through the nonstoichiometric SiC bus/ring waveguide resonator. (b) Single bit PRZ-OOK shapes of the on-resonant intensive optical pump and the on-resonant intensity modulated probe signals at different operating wavelengths.

DOI: 10.1021/acsphotonics.6b00016
ACS Photonics 2016, 3, 806−818

$$T(z, \Delta\Phi) = 1 - \frac{4\Delta\Phi z/z_0}{(1 + (z/z_0)^2)(9 + (z/z_0)^2)} = 1 - \frac{4n_2 k_0 I_{peak} L z/z_0}{(1 + (z/z_0)^2)(9 + (z/z_0)^2)} \quad (5)$$

where $\Delta\Phi$, n_2, and k_0 denote the phase shift, the nonlinear refractive index, and the wavenumber, respectively. As a result, the nonlinear refractive index of nonstoichiometric SiC film is calculated as 2.4×10^{-12} cm^2/W, whereas that of the stoichiometric SiC is determined as 8×10^{-13} cm^2/W. This elucidates the contribution of Si-QDs to the enhanced optical nonlinearity of the Snonstoichiometric SiC. Such a significant increase of n_2 for the nonstoichiometric SiC is correlated with the strong quantum confinement effect occurred in the buried polycrystalline Si-QDs.[6]

Nonlinear All-Optical Kerr Switching of the Non-stoichiometric SiC Ring Waveguide Resonator. The on-resonance wavelength conversion in the nonstoichiometric SiC-based bus/ring waveguide module based on the nonlinear Kerr effect is shown in Figure 11. The unmodulated optical probe signal and the pulsed data embedded optical pump at different wavelengths in same optical telecommunication band are passing through the nonstoichiometric SiC bus/ring waveguide through a 50/50 2 × 1 optical coupler in connection with a lensed fiber. By transmitting the high-power optical pulsed data-stream at any notched wavelength in the transmission spectrum of the nonstoichiometric SiC ring waveguide, all of the resonant dips in the transmittance spectrum can be concurrently red-shifted with the presence of the intensive pump data patterns.

Such a nonlinear Kerr effect causes the refractive index of the nonstoichiometric SiC increased to shift the notched resonant dip by 0.07 nm away from its original wavelength. As a result, the continuous-wave (CW) optical probe signal at a wavelength coincident with another resonant dip is cross-wavelength intensity modulated by the nonlinear optical Kerr effect induced red-shift on transmission resonance dip, which experiences an encoding with its format and sign identical with that of the pump data stream, as shown in Figure 11.

To experimentally implement the ultrafast nonlinear all-optical Kerr wavelength conversion at optical telecommunication wavelengths in the nonstoichiometric SiC bus/ring waveguide resonator, the transient optical pump with a PRZ-OOK data-stream at bit rate of 12 Gbit/s is employed to determine the switching speed on the wavelength shift of the notched transmission dip in the nonstoichiometric SiC ring waveguide resonator. To clearly indicate the format preserved wavelength conversion of the data-stream at different probe wavelength, the Figure 12 shows the waveforms of a single pulsed RZ bit-shape in time domain for the cross-wavelength modulated probe signals probed at different operating wavelengths. At the wavelength of 1559.57 nm, the probe beam can be directly cross-wavelength intensity modulated by the original optical pump data patterns. However, the cross-wavelength intensity modulation efficiency gradually degrades when slightly detuning the probe wavelength away from the transmittance notch, providing that the amplitude of the data bit converted to the probe beam is gradually decreased with the slightly deviated probe wavelength. As evidence, the extinction ratio eventually attenuates to nearly 0 dB when the probe wavelength is detuned to half the red-shift of the notched dip, as induced by the intensive pump in the nonstoichiometric SiC ring waveguide resonator. These observations conclude that the wavelength conversion results

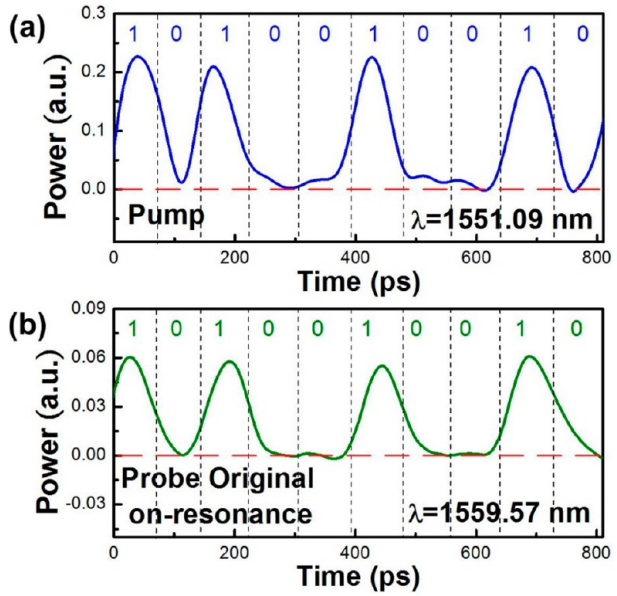

Figure 12. (a) Pump input at the on-resonant dip of λ = 1551.09 nm. (b) Probe output at another on-resonant dip of λ = 1559.57 nm.

from the nonlinear Kerr effect induced resonance red-shift. Theoretically, the allowable switching speed of the ring waveguide resonator is limited by its photon lifetime, which can be expressed from the observed quality factor by $\tau_p = Q/2\pi\nu_0$, where ν_0 represents the central frequency of the resonance dip. With the quality factor of $Q = 2.28 \times 10^4$ at wavelength of 1550 nm, the photon lifetime of about 18.65 ps can guarantee the high-speed intensity modulation in the nonstoichiometric SiC ring waveguide resonator with its maximal modulation speed of ~50 Gbit/s. To further demonstrate the practical PRZ-OOK modulation, which is one of the formats commonly used in the real optical communication network, the optical PRZ-OOK data-stream delivered by the intensive pump is employed for subsequent data transmission analysis.

Figure 12a shows the PRZ-OOK data-stream of the optical pump by externally modulating the continuous-wave laser at 1551.09 nm with the electrical data-stream of AWG. After the cross-wavelength intensity modulation, the corresponding PRZ-OOK data-stream of the probe at another on-resonant dip (1559.57 nm) is demonstrated in Figure 12b. Comparing with the high-power 12-Gbit/s PRZ-OOK pump data-stream, the wavelength-converted probe data-stream can perfectly matched with the optical pump one in time-domain without any delay.

Off-Resonance Wavelength Converter with Format Inverted Data Stream. On the other hand, the wavelength converted and format inverted data stream can also be performed with the same nonstoichiometric SiC bus/ring waveguide resonator by simply coinciding the wavelength of probe with that of the new notched dip red-shifted by the intense optical pump. When the probe beam is located at a wavelength deviated from the notch point, the original transmittance of the probe beam is high. However, the transmittance is suddenly dropped to the minimum when the probe wavelength is exactly matched with the new notch dip formed under the high-power pumped condition, as shown in Figure 13a.

Note that the probe wavelength has to be detuned with exactly the shift caused by the optical pump, otherwise the extinction of the format inverted data will be degraded seriously. To experimentally characterize the high-speed nonlinear all-optical

DOI: 10.1021/acsphotonics.6b00016
ACS Photonics 2016, 3, 806−818

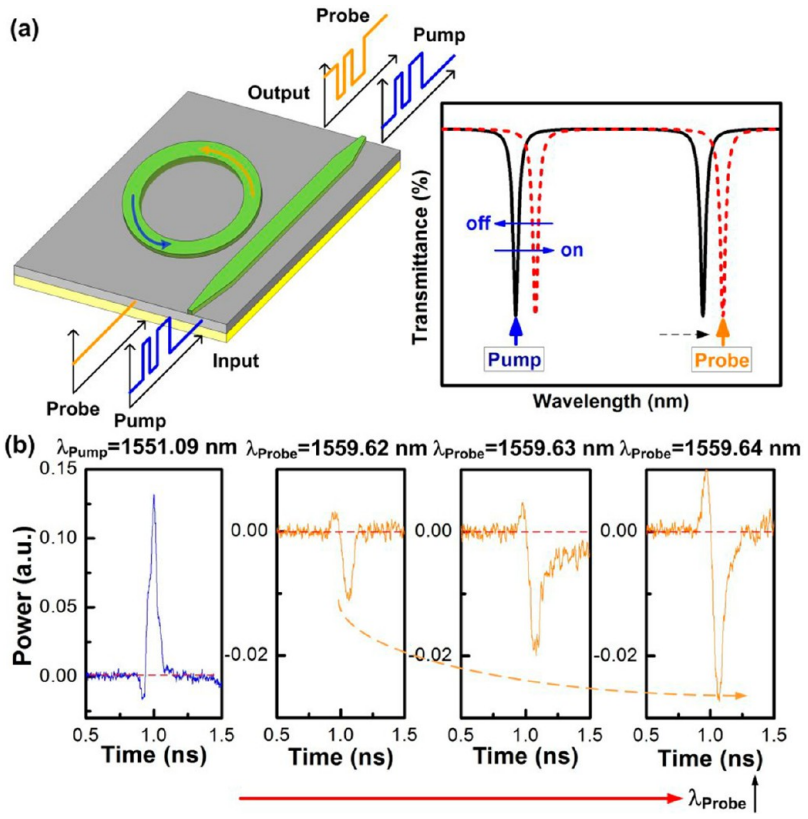

Figure 13. (a) Illustration on the operating principle of the nonlinear optical Kerr effect induced data inversion. (b) Single-bit RZ-OOK data shapes of the on-resonant high-power optical pump and the format-inverted off-resonant probe at different operating wavelengths.

Kerr data switching induced inversion at optical telecommunication wavelengths in the nonstoichiometric SiC bus/ring waveguide resonator, the wavelength of probe beam is shifted from 1559.57 to 1559.64 nm that is corresponding to the wavelength of the newly shifted notch dip for maximizing the inverted data amplitude. At the wavelength ranged between 1559.62 and 1559.64 nm, the probe beam is inversely modulated by the intensive optical pump data patterns, as shown in Figure 13b.

The extracted waveforms of the PRZ-OOK data patterns of pump and probe at 12 Gbit/s are shown in Figure 14. With precisely controlling the wavelength of probe to coincide with the new notch dip shifted to the off-resonant region, the data-stream carried by the optical pump can be perfectly converted to the off-resonant probe with a inverted format. Note that the data inversion can instantly follow up the change on the nonlinear refractive index of the nonstoichiometric SiC that is governed by the nonlinear Kerr effect switching. With the ultrafast all-optical nonlinear Kerr effect based cross-amplitude data follower and inverter, the nonstoichiometric SiC bus/ring waveguide resonator shows the capability of serving as the high-speed device in the future all-optical data processing for chip-level interconnected communication.

When employing the nonlinear Kerr switching effect to convert and invert the waveform of high-speed data in the future all-optical integrated circuits for interconnected communication, it is important to further check the transmission performance of the nonstoichiometric SiC bus/ring waveguide based all-optical data format follower and inverter. The eye-diagram of the 12-Gbit/s PRZ-OOK data-stream before and after wavelength conversion is shown in Figure 15. From the measured eye-

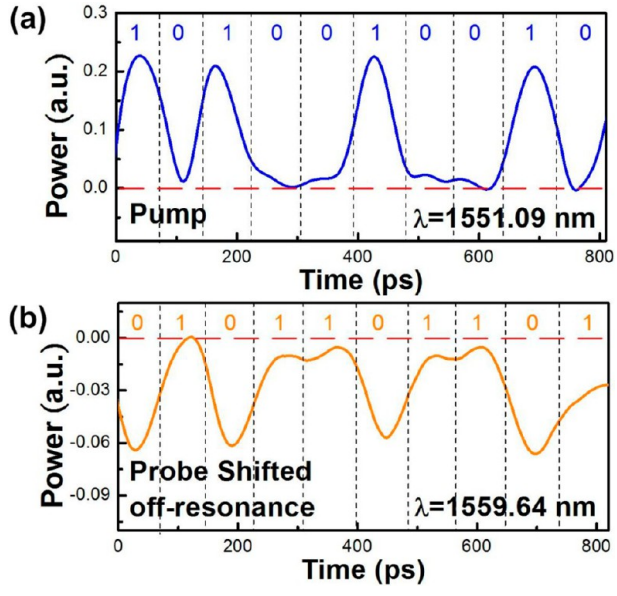

Figure 14. Extracted PRZ-OOK data streams of (a) pump (at λ = 1551.09 nm, on resonance) and (b) probe (at λ = 1559.64 nm, off-resonance) at a bit rate of 12 Gbit/s.

opening diagram, the signal-to-noise ratios (SNR) of the received optical pump and probe data patterns are 12 and 9.4 dB, respectively, leading to a receiving power penalty degraded by 2.6 dB. In addition, the root-mean-square timing jitter measured by the communication analyzer also concurrently degrades from 13 to 22.1 ps after converting the data pattern from pump to probe. The corresponding rising/falling time of the pump signal and

DOI: 10.1021/acsphotonics.6b00016
ACS Photonics 2016, 3, 806−818

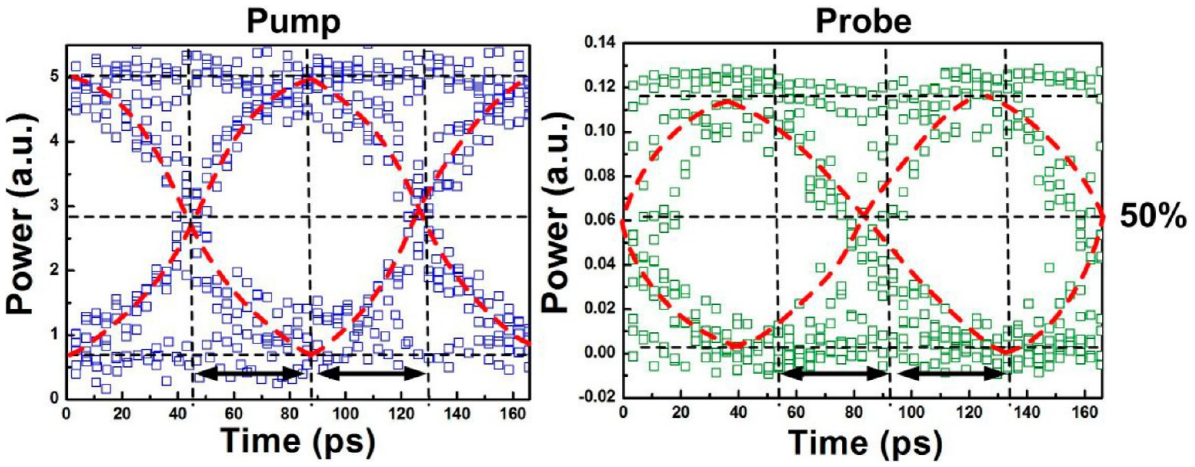

Figure 15. Analyzed eye diagrams of the 12 Gbit/s PRZ-OOK data patterns output from the nonstoichiometric SiC bus/ring waveguide based data format follower/inverter, as detected at on-resonant pump wavelength of λ = 1551.09 nm (left) and at off-resonant probe wavelength of λ = 1559.64 nm (right).

converted probe signal are obtained as 40 and 43 ps, indicating that the modulated probe signal is converted by the pump pulse without distortion.

To neglect the bending loss induced by the nonstoichiometric SiC bus/ring waveguide resonator, we have initially designed the radius of ring waveguide resonator as 150 μm. Actually, the radius of the ring waveguide resonator can be shrunk to ~10 μm, but the propagation loss is inevitably increased. Nevertheless, the propagation loss can be further decreased once optimizing the fabrication process of the ring waveguide resonator. Once the sidewall of the optical waveguide is further optimized, the quality factor of the ring waveguide resonator can be enhanced. The optical power can be effectively enlarged in the ring waveguide resonator with smaller injecting power. Regarding the necessity of peak pump power of up to 3 W, the most efficient way is to further reduce the effective core area of the waveguide for enhancing the peak intensity of incoming pump signal. For instance, the optical intensity can be strongly enhanced by introducing the slot waveguide structure.[38] The effective mode area of slot waveguide structure is much smaller than the channel waveguide, and the optical intensity effectively enhances in the slot waveguide by comparing to the channel waveguide with same injected optical power. That is, the more efficient and compact ultrafast all-optical modulation by using the non-stoichiometric SiC ring waveguide resonator would be realized.

Through PECVD at low temperatures, such structures made by similar group IV semiconductor materials have already shown their CMOS compatibility. For example, the silicon-based optical modulator can be integrated with CMOS chips.[39,40] Della Corte et al. utilized the amorphous silicon (a-Si) to form the photonic devices,[39] and several kinds of effects including photon-induced absorption, thermo-optic and electro-optic mechanisms have been employed to modulate the signal.[39] Rao and co-workers used a-Si material to fabricate the Mach−Zehnder electro-optic modulator with a switching time as short as 2.3 ns.[40] In this work, the nonlinear optical Kerr effect is employed to modulate the signal, which can easily achieve the ultrafast modulation. On the other hand, the nonlinear refractive index of the nonstoichiometric SiC layer is higher than that of the a-Si to enhance the modulation depth. Moreover, in reviewing previous works on studying the optical nonlinearity of a-Si, it is noted that Narayanan has already demonstrated the self-phase modulation in an a-Si waveguide by injecting ultrashort laser pulses. The nonlinear refractive index of a-Si was determined as 4.2×10^{-13} cm^2/W with a TPA coefficient of 4.1 cm/GW at wavelength of 1550 nm.[41] Furthermore, the a-Si based all-optical switch with the use of Kerr effect have also been investigated.[42] However, the TPA mechanism inevitably induces free-carriers in the a-Si waveguide, which not only limits the modulation speed but also distort the modulation traces of the data stream switched by the a-Si based all-optical modulator.[42] Although the TPA-induced FCA can be suppressed by decreasing the pump power injected into the a-Si based devices, the TPA coefficient still enlarges when operating at short wavelength.[43] That is, the operation bandwidth of a-Si based devices is limited by its low bandgap energy property. On the contrary, the present Si-QD doped nonstoichiometric SiC matrix shows great optical nonlinearity as compared to a-Si. By taking the advantage on large bandgap energy of nonstoichiometric SiC host matrix, the TPA-free characteristic of the nonstoichiometric SiC can be maintained even at a peak intensity of up to 0.4 GW/cm^2 at 1550 nm. Even operating at wavelength as short as 800 nm, the obtained TPA coefficient of 0.37 cm/GW is still much lower than that of a-Si at 1550 nm. Furthermore, the nonlinear refractive index of nonstoichiometric SiC can be significantly enhanced to 2.4×10^{-12} cm^2/W at 800 nm by introducing Si-QD dopants into the host matrix, which is enlarged by 1 order of magnitude as compared to that of a-Si. Based on the aforementioned discussions, the Si-QD-doped nonstoichiometric SiC can be regarded as a suitable nonlinear optical material in developing ultrafast Kerr switch for all-optical modulation.

CONCLUSION

By using the PECVD grown nonstoichiometric SiC film as a core layer in the channel waveguide, the SiO_2/nonstoichiometric SiC/SiO_2 bus/ring waveguide resonator can function as an ultrafast optical switch based on the nonlinear Kerr effect for dual-functional wavelength and data-format conversions. By employing a pump signal with a peak intensity of 35.3 mW/μm^2 into a 50/50 coupler with a coupling loss of 5-dB, the nonlinear Kerr coefficient of the nonstoichiometric SiC is determined as $n_2 = \delta n_g / I_{cir} = 3.14 \times 10^{-13}$ cm^2/W at a wavelength of 1550 nm. Owing to the strong quantum confinement occurred in buried polycrystalline Si-QDs, the nonstoichiometric SiC reveals a large increment on its nonlinear refractive index under intensive

DOI: 10.1021/acsphotonics.6b00016
ACS Photonics 2016, 3, 806−818

pumping. The 300 nm thick nonstoichiometric SiC film on a 3 μm thick SiO_2 coated Si wafer grown with the fluence ratio of $R = [CH_4]/([SiH_4] + [CH_4]) = 0.5$ reveals a Si/C atomic concentration ratio of 2.37. In comparison with the stoichiometric SiC, the $SiC_{0.42}$ enlarges its excessive Si concentration by 37.2%. The Raman scattering spectral peak shows Si-QDs with sizes ranging between 2 and 3 nm. The quality factor of the ring waveguide resonator is as high as $Q = 2.28 \times 10^4$ and the transmittance drop is nearly 60% at 1551.08 nm with a notching spacing of $\delta\lambda = 1.04$ nm.

The intensive optical pump data patterns cause a cross-wavelength modulation on the probe, and the modulation depth is gradually decreased by the transient red-shift on the probe wavelength. The wavelength shift related to the maximal amplitude of the data-inverted probe signal is up to 0.07 nm, as contributed by the nonlinear optical Kerr effect induced refractive index change. In application, the optical PRZ-OOK data-stream at a bit rate of up to 12 Gbit/s can be either wavelength converted or format inverted from pump to probe by carefully adjusting the wavelength of probe to be coincident with or aside near the notched transmission point of the non-stoichiometric SiC ring waveguide resonator. The wavelength-converted probe data-stream can perfectly match with the pump data stream without any delay in time domain. From the measured eye-opening diagram, the SNR of 9.4 dB for the data transferred to the probe is only degraded by 2.6 dB after wavelength conversion and format inversion. A slight degradation on the rms timing jitter enlarged from 13 to 22.1 ps is also observed due to the noise added during recovery. The corresponding rising and falling times of the pump and converted probe signals are obtained as 40 and 43 ps, respectively, indicating that the modulated probe signal is converted by the pump pulse without distortion.

AUTHOR INFORMATION

Corresponding Author

*Phone: +886-2-33663700, ext. 6519. Fax: +886-2-33669598. E-mail: grlin@ntu.edu.tw.

Notes

The authors declare no competing financial interest.

ACKNOWLEDGMENTS

Financial support from the Ministry of Science and Technology, Taiwan, R.O.C., and the Excellent Research Projects of National Taiwan University, Taiwan, R.O.C., under Grants MOST-103-2221-E002-042-MY3, MOST-104-2221-E-002-117-MY3, NTU-ERP-105R89081, and NTU-ERP-105R89083 are acknowledged.

REFERENCES

(1) Wu, C.-L.; Su, S.-P.; Lin, G.-R. All-optical data inverter based on free-carrier absorption induced cross-gain modulation in Si quantum dot doped SiO_x waveguide. *IEEE J. Sel. Top. Quant. Electron.* **2014**, *20*, 1−9.

(2) Navarro-Urrios, D.; Pitanti, A.; Daldosso, N.; Gourbilleau, F.; Rizk, R.; Pucker, G.; Pavesi, L. Quantification of the carrier absorption losses in Si-nanocrystal rich rib waveguides at 1.54 μm. *Appl. Phys. Lett.* **2008**, *92*, 051101.

(3) Creazzo, T.; Redding, B.; Marchena, E.; Shi, S.; Prather, D. W. Free-carrier absorption modulation in silicon nanocrystal slot waveguides. *Opt. Lett.* **2010**, *35*, 3691−3693.

(4) Wu, C.-L.; Su, S.-P.; Lin, G.-R. All-optical modulation based on silicon quantum dot doped SiOx:QD waveguide. *Laser Photon. Rev.* **2014**, *8*, 766−776.

(5) Martínez, A.; Blasco, L.; Sanchis, P.; Galán, J. V.; García-Rupérez, J.; Jordana, E.; Gautier, P.; Lebour, Y.; Hernández, S.; Spano, R.; Guider, R.; Daldosso, N.; Garrido, B.; Fedeli, J. M.; Pavesi, L.; Martí, J. Ultrafast all-optical switching in a silicon-nanocrystal-based silicon slot waveguide at telecom wavelengths. *Nano Lett.* **2010**, *10*, 1506−1511.

(6) Takagahara, T.; Takeda, K. Theory of the quantum confinement effect on excitons in quantum dots of indirect-gap materials. *Phys. Rev. B: Condens. Matter Mater. Phys.* **1992**, *46*, 15578−15581.

(7) Imakita, K.; Ito, M.; Fujii, M.; Hayashi, S. Nonlinear optical properties of Si nanocrystals embedded in SiO_2 prepared by a cosputtering method. *J. Appl. Phys.* **2009**, *105*, 093531.

(8) Zhang, P.; Zhang, X.; Xu, J.; Mu, W.; Xu, J.; Li, W.; Chen, K. Tunable nonlinear optical properties in nanocrystalline Si/SiO_2 multilayers under femtosecond excitation. *Nanoscale Res. Lett.* **2014**, *9* (1), 28.

(9) Wu, C.-L.; Lin, Y.-H.; Cheng, C.-H.; Su, S.-P.; Huang, B.-J.; Chang, J.-H.; Wu, C.-I; Lee, C.-K.; Lin, G.-R. Enriching Si quantum dots in a Si-rich SiNx matrix for strong $\chi^{(3)}$ optical nonlinearity. *J. Mater. Chem. C* **2016**, *4*, 1405−1413.

(10) Lin, G.-R.; Su, S.-P.; Wu, C.-L.; Lin, Y.-H.; Huang, B.-J.; Wang, H.-Y.; Tsai, C.-T.; Wu, C.-I; Chi, Y.-C. Si-rich SiN_x based Kerr switch enables optical data conversion up to 12 Gbit/s. *Sci. Rep.* **2015**, *5*, 09611.

(11) Tsang, H. K.; Wong, C. S.; Liang, T. K.; Day, I. E.; Roberts, S. W.; Harpin, A.; Drake, J.; Asghari, M. Optical dispersion, two-photon absorption and self-phase modulation in silicon waveguides at 1.5 μm wavelength. *Appl. Phys. Lett.* **2002**, *80*, 416−418.

(12) Edmond, J. A.; Kong, H. S.; Carter, C. H., Jr Blue LEDs, UV photodiodes and high-temperature rectifiers in 6H-silicon carbide. *Phys. B* **1993**, *185*, 453.

(13) Morkoç, H.; Strite, S.; Gao, G. B.; Lin, M. E.; Sverdlov, B.; Burns, M. Large-band-gap SiC, III-V nitride, and II-VI ZnSe-based semiconductor device technologies. *J. Appl. Phys.* **1994**, *76* (3), 1363−1398.

(14) Cheng, C. H.; Wu, C.-L.; Chen, C.-C.; Tsai, L.-H.; Lin, Y. H.; Lin, G.-R. Si-rich SiC light-emitting diodes with buried Si quantum dots. *IEEE Photonics J.* **2012**, *4*, 1762−1775.

(15) Tai, H.-Y.; Cheng, C.-H.; Lin, G.-R. Blue-green light emission from Si and SiC quantum dots co-doped Si-rich SiC p-i-n junction diode. *IEEE J. Sel. Top. Quant. Electron.* **2014**, *20*, 1−7.

(16) Tawada, Y.; Tsuge, K.; Kondo, M.; Okamoto, H.; Hamakawa, Y. Properties and structure of SiC:H for high-efficiency-Si solar cell. *J. Appl. Phys.* **1982**, *53*, 5273−5281.

(17) Song, D.; Cho, E. C.; Conibeer, G.; Flynn, C.; Huang, Y.; Green, M. A. Structural, electrical and photovoltaic characterization of Si nanocrystals embedded SiC matrix and Si nanocrystals/c-Si heterojunction devices. *Sol. Energy Mater. Sol. Cells* **2008**, *92*, 474−481.

(18) Lee, C.-T.; Tsai, L.-H.; Lin, Y.-H.; Lin, G.-R. A chemical vapor deposited silicon rich silicon carbide p−n junction based thin-film photovoltaic solar cell. *ECS J. Solid State Sci. Technol.* **2012**, *1*, Q144−Q148.

(19) Cheng, C.-H.; Lin, Y.-H.; Chang, J.-H.; Wu, C.-I.; Lin, G.-R. Semi-transparent Si-rich SiC p-i-n photovoltaic solar cell grown by hydrogen-free PECVD. *RSC Adv.* **2014**, *4*, 18397−18405.

(20) Casady, J. B.; Johnson, R. W. Status of silicon carbide (SiC) as a wide-bandgap semiconductor for high-temperature applications: A review. *Solid-State Electron.* **1996**, *39*, 1409−1422.

(21) Ruddy, F. H.; Dulloo, A. R.; Seidel, J. G.; Seshadri, S.; Rowland, L. B. Development of a silicon carbide radiation detector. *IEEE Trans. Nucl. Sci.* **1998**, *45*, 536−541.

(22) Seshadri, S.; Dulloo, A. R.; Ruddy, F. H.; Seidel, J. G.; Rowland, L. B. Demonstration of an SiC neutron detector for high-radiation environments. *IEEE Trans. Electron Devices* **1999**, *46*, 567−571.

(23) Zhuang, H.; Yang, N.; Zhang, L.; Fuchs, R.; Jiang, X. Electrochemical properties and applications of nanocrystalline, microcrystalline, and epitaxial cubic silicon carbide films. *ACS Appl. Mater. Interfaces* **2015**, *7*, 10886−10895.

(24) Lefèvre, J.; Costantini, J. M.; Esnouf, S.; Petite, G. SiC and Si quantum dots co-precipitated Si-rich SiC film with n- and p-type dopants grown by hydrogen-free PECVD. *J. Appl. Phys.* **2009**, *106*, 083509.

(25) Cheng, C.-H.; Wu, C.-L.; Lin, Y.-H.; Yan, W.-L.; Shih, M.-H.; Chang, J.-H.; Wu, C.-I; Lee, C.-K.; Lin, G.-R. Strong optical nonlinearity

DOI: 10.1021/acsphotonics.6b00016
ACS Photonics 2016, 3, 806−818

of the nonstoichiometric silicon carbide. *J. Mater. Chem. C* **2015**, *3*, 10164−10176.
(26) Lin, G.-R.; Lin, C.-J.; Yu, K.-C. Time-resolved photoluminescence and capacitance-voltage analysis of the neutral vacancy defect in silicon implanted SiO_2 on silicon substrate. *J. Appl. Phys.* **2004**, *96*, 3025−3027.
(27) Zi, J.; Büscher, H.; Falter, C.; Ludwig, W.; Zhang, K.; Xie, X. Raman shifts in Si nanocrystals. *Appl. Phys. Lett.* **1996**, *69*, 200−202.
(28) Faraci, G.; Gibilisco, S.; Russo, P.; Pennisi, A. R.; La Rosa, S. Modified Raman confinement model for Si nanocrystals. *Phys. Rev. B: Condens. Matter Mater. Phys.* **2006**, *73*, 033307.
(29) Wu, C.-L.; Lin, G.-R. Power Gain Modeling of Si quantum dots embedded in a SiO waveguide amplifier with inhomogeneous broadened spontaneous emission. *IEEE J. Sel. Top. Quantum Electron.* **2013**, *19*, 1−9.
(30) Yariv, A. Universal relations for coupling of optical power between micro resonators and dielectric waveguides. *Electron. Lett.* **2000**, *36*, 321−322.
(31) Della Corte, F. G.; Cocorullo, G.; Iodice, M.; Rendina, I. Temperature dependence of the thermo-optic coefficient of InP, GaAs, and SiC from room temperature to 600 K at the wavelength of 1.5 μm. *Appl. Phys. Lett.* **2000**, *77*, 1614−1616.
(32) Almeida, V. R.; Lipson, M. Optical bistability on a silicon chip. *Opt. Lett.* **2004**, *29*, 2387−2389.
(33) Della Corte, F. G.; Rao, S.; Coppola, G.; Summonte, C. Electro-optical modulation at 1550 nm in an as-deposited hydrogenated amorphous silicon p-i-n waveguiding device. *Opt. Express* **2011**, *19*, 2941−2951.
(34) López-Suárez, A.; Torres-Torres, C.; Rangel-Rojo, R.; Reyes-Esqueda, J. A.; Santana, G.; Alonso, J. C.; Ortiz, A.; Oliver, A. Modification of the nonlinear optical absorption and optical Kerr response exhibited by nc-Si embedded in a silicon-nitride film. *Opt. Express* **2009**, *17*, 10056−10068.
(35) Huang, R.; Chen, K.; Han, P.; Dong, H.; Wang, X.; Chen, D.; Li, W.; Xu, J.; Ma, Z.; Huang, X. Strong green-yellow electroluminescence from oxidized amorphous silicon nitride light-emitting devices. *Appl. Phys. Lett.* **2007**, *90*, 093515−093513.
(36) DesAutels, G. L.; Brewer, C.; Walker, M.; Juh, S.; Finet, M.; Ristich, S.; Whitaker, M.; Powers, P. Femtosecond laser damage threshold and nonlinear characterization in bulk transparent SiC materials. *J. Opt. Soc. Am. B* **2008**, *25*, 60−66.
(37) Chen, R.; Lin, D. L.; Mendoza, B. Enhancement of the third-order nonlinear optical susceptibility in Si quantum wires. *Phys. Rev. B: Condens. Matter Mater. Phys.* **1993**, *48*, 11879−11882.
(38) Rukhlenko, I. D.; Premaratne, M.; Agrawal, G. P. Effective mode area and its optimization in silicon-nanocrystal waveguides. *Opt. Lett.* **2012**, *37*, 2295−2297.
(39) Della Corte, F. G.; Rao, S. Use of amorphous silicon for active photonic devices. *IEEE Trans. Electron Devices* **2013**, *60*, 1495−1505.
(40) Rao, S.; Coppola, G.; Gioffrè, M. A.; Della Corte, F. G. A 2.5 ns switching time MachZehnder modulator in as-deposited a-Si:H. *Opt. Express* **2012**, *20*, 9351−9356.
(41) Pelc, J. S.; Rivoire, K.; Vo, S.; Santori, C.; Fattal, D. A.; Beausoleil, R. G. Picosecond all-optical switching in hydrogenated amorphous silicon microring resonators. *Opt. Express* **2014**, *22*, 3797−3810.
(42) Narayanan, K.; Preble, S. F. Optical nonlinearities in hydrogenated- amorphous silicon waveguides. *Opt. Express* **2010**, *18*, 8998−9005.
(43) Vukovic, N.; Healy, N.; Suhailin, F. H.; Mehta, P.; Day, T. D.; Badding, J. V.; Peacock, A. C. Ultrafast optical control using the Kerr nonlinearity in hydrogenated amorphous silicon microcylindrical resonators. *Sci. Rep.* **2013**, *3*, 2885.

DOI: 10.1021/acsphotonics.6b00016
ACS Photonics 2016, 3, 806−818